ELSEVIER

Chemical Engineering Journal 135S (2008) S309–S316

Chemical Engineering Journal

www.elsevier.com/locate/cej

Transparent silicon/glass microreactor for high-pressure and high-temperature reactions

Franz Trachsel, Cédric Hutter, Philipp Rudolf von Rohr *

Institute of Process Engineering, Sonneggstrasse 3, ETH Zurich, 8092 Zurich, Switzerland

Abstract

To increase mass transfer in solid catalyzed gas–liquid hydrogenations, the reactions are often operated at high pressures. Silicon/glass microreactors present a possibility to safely handle high-pressure and provide optical access into the reaction channel for flow investigations. In this study we present a Si/glass microreactor with soldered microfluidic connections for high-pressure and high-temperature applications. Mechanical testing of the device by tensile and pressure tests showed no failure for continuous operation at 140 bar and 80 °C. The improved microreactor design is applied for a well-described solid catalyzed exothermic hydrogenation at operating conditions up to 51 bar and 71 °C. Additionally the two-phase gas–liquid flow is investigated in the microreactor. Results clearly indicated the improvement of the reaction rate from 0.004 mol g_{cat}^{-1} min^{-1} at ambient conditions to 0.046 mol g_{cat}^{-1} min^{-1} at 51 bar and 71 °C. The reaction was observed to be mass transfer limited.

Keywords: High-pressure; High-temperature; Microreactor; Microfluidic connection; Hydrogenation

1. Introduction

Microreactors have several advantages compared to their macroscale counterparts [1–3]. A high surface-area-to-volume ratio (4–5 orders of magnitude greater than a conventional batch reactor) enhances heat and mass transfer. Temperature control of strongly exothermic chemical reactions is improved due to the small hold up, high heat transfer rates to the channel walls and by the relatively high heat capacity of the channel walls compared to the heat supplied by the reaction mixture. The partial or total elimination of hot spots enhances process safety by avoiding thermal runaway. An additional advantage of the small length scale of these microfluidic systems is their potential for high-pressure applications due to lower mechanical stress in the reactor material.

In this study we use the case of a multiphase heterogeneously catalyzed hydrogenation to focus on two aspects of the microreactor system: the analysis and testing of soldered microfluidic connections to Si/glass microreactors, and the feasibility of their application in high-pressure and high-temperature chemical reaction engineering. First, the mechanical strength of the microfluidic connections and the whole microreactor device is analyzed by tensile and pressure tests. Second, the heterogeneously catalyzed hydrogenation of cyclohexene is conducted in a T-shaped packed bed microreactor as a model reaction. The influence of pressure and temperature on the reaction rate is investigated. Optical access into the reaction chamber allows the observation of crucial parameters such as flow patterns, catalyst packing and mixing of the reactants.

1.1. Microfluidic connections

Microfluidic devices have developed unique solutions for the fluidic connection to devices such as pumps or analytical systems. High-pressure and high-temperature fluidic connections for Si/glass microreactors are rarely reported. But the use of Si/glass microreactors has several advantages compared to metallic, glass or plastic devices. Standard cleanroom fabrication allows precise micromachining of microreactor features. Also silicon and glass are resistant to corrosion from most chemical species except strong acids. Optical access is important for the investigation of mixing, flow characteristics [4] and residence time distribution [5]. One of the main disadvantages is the brittle mechanical behaviour of silicon and glass, which makes it difficult to handle the devices and attach microfluidic connections to it.

Two major methods exist for making microfluidic connections on microreactor chips: integrated connections and modular connections [6].

* Corresponding author. Tel.: +41 44 632 24 88; fax: +41 44 632 15 01.
E-mail address: vonrohr@ipe.mavt.ethz.ch (P.R. von Rohr).

1385-8947/$ – see front matter © 2007 Elsevier B.V. All rights reserved.
doi:10.1016/j.cej.2007.07.049

Integrated connections are directly attached microfluidic connections. The major disadvantages of this connection type are the complicated fabrication procedure and the resulting dead volume, which is not easily accessible. Press fittings with fused silica capillaries in etched holes are used for pressures up to 34 bar [7]. A theoretical value of 66 bar is achievable with an integrated flange and peek tubing [8]. Directly epoxy-glued connections for pressures up to 137 bar are presented by Spiering et al., Pattekar and Kothare and Andersson et al. [9–11]. High-temperature glass sealing of Kovar for pressures up to 125 bar and temperatures up to 1300 °C has been demonstrated by micro power systems [12]. The anodic bonding of Kovar to borosilicate glass is reported by Blom et al. [13], who derives a theoretical value of 200 bar from tensile tests.

Modular connections consist of reusable parts. A housing in which the microreactor is embedded provides leak tight connections. A precise alignment of the connecting components is needed. PEEK housing and fittings are used by Nittis et al. [14] up to 6 bar pressure. An integrated rubber o-ring for sealing up to 5.5 bar is shown by Yao et al. [15].

Commercially available microfluidic connection interfaces have pressure ranges from 50 bar [16] to 100 bar [17].

Metallic and glass solder has been used for microfluidic connections by Ratner et al. [18] and Yen et al. [19]. A mechanical characterization of soldered microfluidic connections has not been reported yet. And no data about temperature dependent mechanical strength of the different microfluidic connections is available. For a robust and easily fabricated microfluidic connection the soldering of a capillary onto a silicon surface is proposed. Press fittings with housings can introduce non-uniform stress on the Si/glass chip reactor and lead to the fracture of the reactor. Glass sealing needs fabrication temperatures far above the anodic bonding temperature, which would result in a weakened bond between silicon and glass and could affect already integrated catalyst or sensors. Anodic bonding of Kovar to glass is time consuming through several additional cleanroom steps.

The characterization of the mechanical strength of soldered microfluidic connection was done by tensile and pressure tests to simulate operating conditions during a high-pressure and high-temperature reaction. The results show that a Si/glass microreactor with soldered fluidic connections is suitable to withstand pressures up to 140 bar and temperatures up to 80 °C. Tensile tests indicate that the forces required to separate microfluidic connections from the microreactor are 1 order of magnitude higher than earlier reported.

1.2. Hydrogenations in microreactors

To present the influence of pressure and temperature on the reaction performance, we investigated the gas–liquid–solid hydrogenation of cyclohexene in a packed bed microreactor using commercially available Pd catalyst. The rate-limiting step is the transport of hydrogen to the catalyst. We chose this model reaction for several reasons: (1) the exothermic character ($\Delta H = -118$ kJ/mol) offers a possibility to show the advantages of microreactors in temperature control, (2) a change in the operating variables (p, T) has significant influence on the reaction rate and (3) this reaction serves as a model for many significant reaction classes in the chemical, process and petroleum industries. It is well described in the literature [20–23].

Recently a number of studies of catalytic hydrogenation [24–27] have been conducted in different types of microreactors [28–30]. Losey et al. studied the hydrogenation of cyclohexene at ambient pressure in porous and packed bed microreactors over Pt catalyst [31,32]. The reaction was found to be mass transfer limited. At temperatures up to 200 °C and ambient pressure Surangalikar et al. and Besser et al. [33,34] conducted the same reaction in the gas phase over sputtered Pt catalyst, where the reaction was limited by the intrinsic reaction rate. Continuous high-pressure hydrogenation reactions in small tube reactors with inner diameters of 1 and 4 mm, respectively have been presented by Desai and co-worker and Yoswathananont et al. [35,36].

2. Experimental

2.1. Microreactor fabrication

A standard photolithography, dry-etching and anodic bonding technique was used for microreactor fabrication. Silicon wafers used were 4 in. p-type, (1 1 1) double side polished with a resistivity of 0.014 Ω cm and 525 μm thickness. A high-

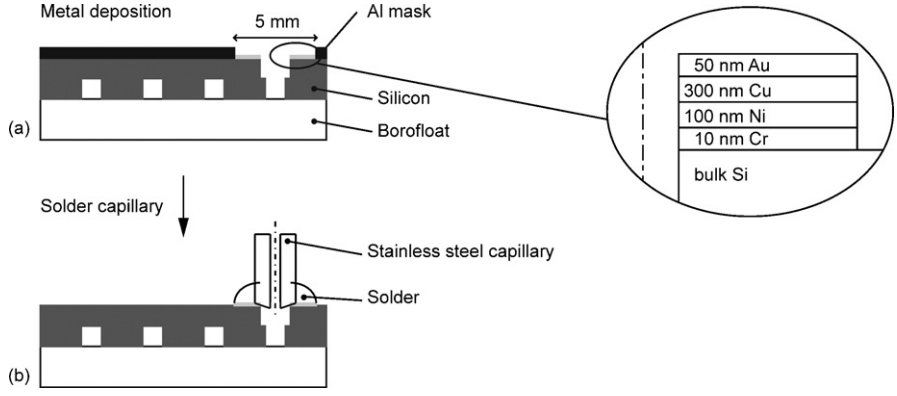

Fig. 1. Schematic of the microfluidic connection fabrication. (a) Thin film metallization using an aluminum shadow mask and electron beam evaporation. (b) Soldered capillary on the backside of the Si/glass microreactor.

resolution transparency foil was used for the photolithographic patterning of the wafer. The dry etching was performed using an inductively coupled plasma (ICP) etching system (Surface Technology Systems). The etch process used resulted in a rectangular channel shape with a depth of approximately 340 μm. A 100 mm diameter borosilicate glass wafer (Borofloat®, Schott) of 700 μm thickness was used to cover the microfluidic channels. Anodic bonding was performed on a substrate bonder (SB6, Süss MicroTec) at 450 °C and a voltage of 1500 V.

2.2. Microfluidic connections

Around the inlet and outlet holes chromium, nickel, copper and gold were subsequently deposited by electron beam evaporation (Pfeifer Vacuum Classic 500) according to Fig. 1(a). A shadow mask was used during the evaporative deposition. Gold is used as the top layer to provide complete wetting with the tin–silver solder. Copper prevents the formation of an oxide layer on the nickel layer. Nickel itself acts as a diffusion barrier. Chromium is the actual undercoating on the silicon surface.

Stainless steel capillaries of 50 mm length (outer diameter = 1.59 mm, inner diameter = 0.5 mm) were turned on one end to provide a slight cone for accurate positioning on the etched inlet and outlet holes. About 5 mm at the end of the tubing was grinded away to remove the oxide layer. After grinding, the capillary was cleaned with acetone and immediately pre-tin-plated with the corresponding flux agent for stainless steels.

The soldering setup consisted of a hot plate and a positioning table. Capillaries were mounted on a drill chuck for precise orthogonal alignment on the microreactor chip. A hot plate and a soldering iron for local heating were used for heating the parts and melting of the solder. Prior to soldering, the capillaries were tinned with flux agent. No plugging of the channel due to flux or solder was observed during fabrication. Fig. 1(b) shows a schematic of the soldered microfluidic connection.

2.3. Mechanical testing

Tensile tests at elevated temperature were performed to simulate the loads on the fluidic connection. The tensile test does not represent the actual load case on the fluidic connection in a pressurized microreactor. The boundary conditions given by the used sample holder and the applied tensile load are not comparable to a simply supported pressurized microreactor. Additionally the modes of failure are not identical. A fluidic connection fails when the first leak appears. Leaks cannot be detected by the tensile test, only the separation of the capillary from the device. However, this test provides an estimation of the maximal strength of the soldered microfluidic connection.

The test specimens were fixed in a holder device, which provides a transmission of force from the capillary to the soldered part of the connection. The holder itself was not fixed completely so that the specimen could move and no moment was introduced on the specimen. Tests were carried out on a mechanical testing machine (Zwick 1474) with a testing temperature range of 5–300 °C and a relative accuracy of ±0.5% at 200 N. To conduct tensile tests at elevated temperatures, a climate chamber was installed around the testing section of the machine. All experiments were performed with a pre-load of 2 N and a test speed of

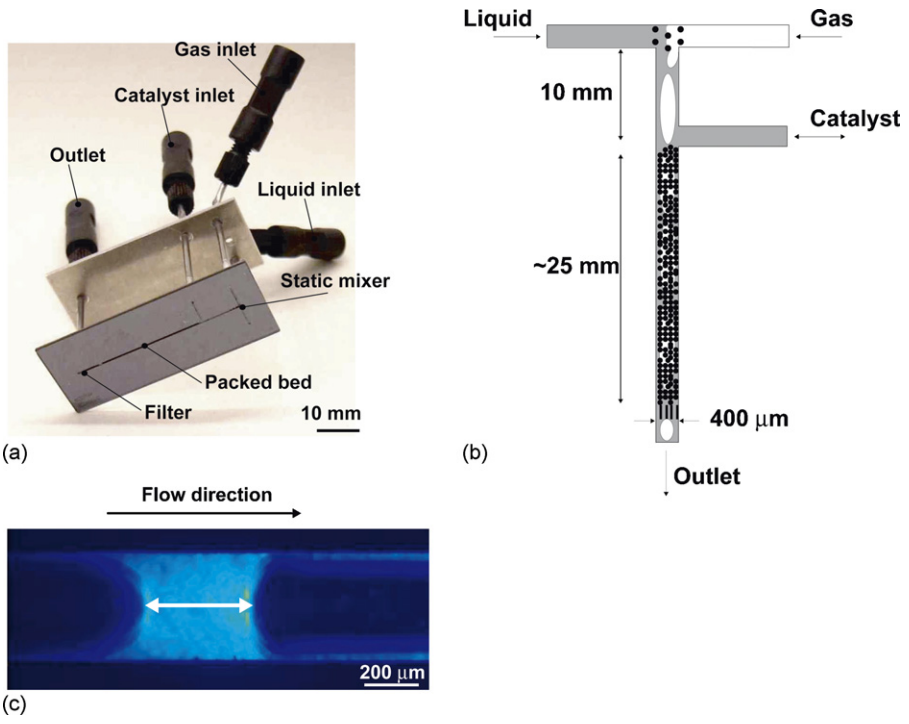

Fig. 2. Microreactor design. (a) Photograph of the Si/glass microreactor. An alumina plate was attached to the capillaries for better handling of the reactor. High-pressure fittings (Upchurch Scientific) were used for the connection with the experimental setup. (b) Schematic of the packed bed microreactor during operation. The catalyst inlet/outlet was closed during operation. (c) Fluorescent micrograph of a liquid slug. The system pressure is 20 bar, $V_L^* = 20$ μL/min and $V_G^* = 20$ mLn/min. Indicated is the measured length of the liquid slug. The channel width is 400 μm.

1 mm/min. The experiment was terminated when the capillary was separated from the silicon surface.

To test the microreactor under pressure and thermal load conditions the microreactor was filled with water, pressurized with nitrogen and placed in a heated water bath.

2.4. Gas–liquid–solid catalyzed hydrogenation of cyclohexene

2.4.1. Microreactor characterization

The continuous solid catalyzed hydrogenation experiments were conducted in a T-shaped microreactor. The reaction took place in a straight 36 mm long single reaction channel 340 μm in depth and 400 μm in width where the catalyst particles were placed. The hydraulic diameter d_H was 370 μm. Inlet and outlet holes were 600 μm in diameter. The gas and liquid streams were fed via two side channels and contacted in a static mixer consisting of etched columns with a diameter of 100 μm and a distance of 100 μm in between. The static mixer induced mixing of the gas and liquid phases. A 10 mm long mixing section enabled the gas and liquid phase to mix completely before entering the packed bed. Fig. 2(a) shows a photograph of the device, and the schematic of the microreactor design is given in Fig. 2(b).

Palladium on silica–alumina particles (2 wt% Pd, Johnson Matthey) was used as the catalyst. After sieving, a well-defined particle size distribution was achieved and a mean particle diameter of 115 μm was measured by laser diffraction spectroscopy (Helos 12KA, Sympatec). The metal surface area to mass ratio was 1.75 m^2/g and the dispersion was 19.7%, measured with pulsed CO chemisorption (Autochem 2910, Micromeritics). The catalyst particles were placed in the microreactor via a side channel by applying a vacuum at the outlet. Filter elements near the common outlet (length = 300 μm, width = 50 μm with 50 μm space in between) prevented the catalyst particles from leaving the microreactor. Ultrasonic treatment was used to generate a random particle distribution in the microchannel. A packed bed structure extended to a length of about 25 mm in the microchannel. This corresponds to a typical catalyst mass of 1.5 mg, which was measured by taking the difference between the measured masses of the empty and filled dried microreactors.

Flow patterns were observed at ambient temperature and pressures ranging from 5 to 50 bar by laser induced fluorescence (LIF) using Rhodamine B as fluorochrome. The fluid pair methanol/nitrogen was used instead of cyclohexene/hydrogen for the flow characterization because of the immiscibility of the Rhodamine B solution in cyclohexene. The capillary numbers, *Ca*, for the reaction mixture and substituted system were 0.0037 and 0.0038, respectively, where $Ca = \eta u/\sigma$, and η denotes the liquid dynamic viscosity, u the bubble velocity and σ is the surface tension. The Reynolds numbers (*Re*) were 73 for cyclohexene/hydrogen and 81 for methanol/nitrogen. The close values of the different *Ca* and *Re* numbers result in the same flow regime for both systems. A typical LIF micrograph of a liquid slug is shown in Fig. 2(c).

2.4.2. Hydrogenation of cyclohexene

The model reaction used was the hydrogenation of cyclohexene over Pd catalyst:

$$C_6H_{10} + H_2 \xrightarrow{Pd} C_6H_{12}. \quad (1)$$

The reaction is exothermic ($\Delta H = -118.8$ kJ/mol). The reaction rate is reported to be half-order with respect to hydrogen and zero-order with respect to cyclohexene [22]. The reaction rate is given by the following equation:

$$r = k c_{H_2}^{l\,1/2}, \quad (2)$$

where k is the reaction rate constant and $c_{H_2}^{l}$ is the concentration of dissolved hydrogen in liquid cyclohexene depending on pressure and temperature. The concentration of hydrogen in cyclohexene can be calculated by Henry's law and varies linearly with pressure in the temperature range of 30–100 °C and in the pressure range of 10–100 bar from 0.0025 to 0.035 mol H_2/mol C_6H_{10} [37].

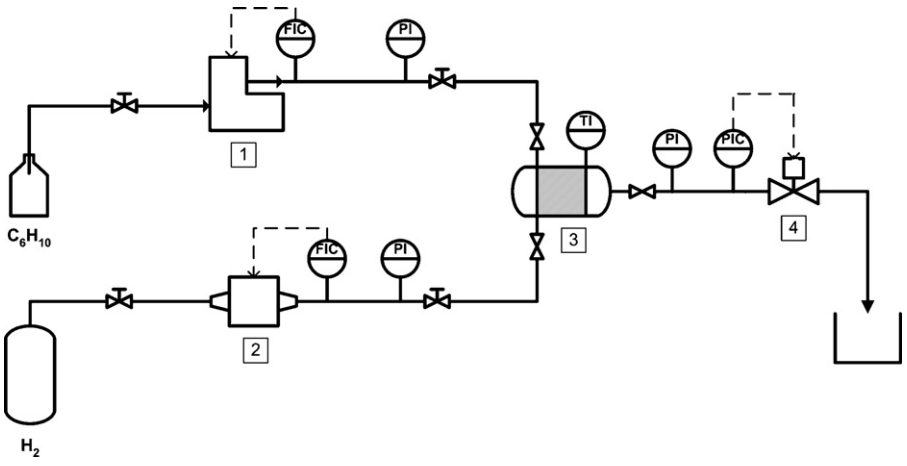

Fig. 3. Schematic of the experimental setup for the high-pressure catalytic hydrogenation of cyclohexene in a packed bed microreactor. (1) High-pressure syringe pump (D260, Isco) for cyclohexene delivery. (2) Mass flow controller for H_2 (F-230M, Bronkhorst). (3) Packed bed microreactor and (4) high-precision back-pressure regulator (BP-1580-81, JASCO). Pressure sensors with an accuracy of ±0.5% were used (Endress & Hauser). Not shown in the schematic are the tubing and instrumentation to flood the setup with nitrogen.

2.4.3. Experimental setup

The schematic of the experimental setup is shown in Fig. 3. It allows a maximum operating pressure of 170 bar. Stainless steel and PEEK (polyetheretherketone) tubing (outer diameter = 1.59 mm, inner diameter = 0.5 mm), valves and interconnections were used for fluid distribution. The microreactor was placed in a heated water bath for experiments at high temperatures and onto a microscope for LIF measurements.

The reaction was conducted at constant superficial velocities of both the gas and the liquid phase. The liquid flow rate was kept constant at 20 μL/min as the liquid phase was assumed to be incompressible. To provide a constant volumetric gas flow rate the mass flow rate was varied with pressure and temperature from 5 mLn/min ($p = 5$ bar, $T = 23\,^{\circ}$C) to 50 mLn/min (50 bar, $T = 23\,^{\circ}$C). The gas mass flow rate was adjusted for higher pressures and temperatures assuming ideal gas conditions. This correction in the gas flow rate changed the stoichiometric factor for the total system from 1.1 ($V_L^* = 20$ μL/min and $V_G^* = 5$ mLn/min at $p = 5$ bar, $T = 23\,^{\circ}$C) to 11.3 ($V_L^* = 20$ μL/min, $V_G^* = 50$ mLn/min, $p = 50$ bar, $T = 23\,^{\circ}$C), where V_i^* is the volumetric flow rate of the liquid and the gas, respectively. Even though the reaction is exothermic, no cooling of the microreactor was needed. A lumped heat transfer coefficient from the microreactor to the environment was measured to be 25 W/(m^2 K). Therefore the heat loss of the microreactor device dominated the heat generation of the reaction above a minimum temperature difference of 4.6 K.

The catalyst was activated with H_2 at 20 bar and ambient temperature for 80 min before each experiment. Using this treatment, the same catalyst activity was maintained for several experiments. Deactivation was also prevented by an in-line peroxide trap containing alumina [38], but no change in catalyst activity was observed due to the short total experiment time.

After reaching steady state flow conditions, product samples were taken after 40, 55 and 90 min. Conversion was analyzed ex-situ by GC–MS and averaged over time for reaction rate calculations.

3. Results and discussion

3.1. Mechanical testing

Three different failure types which occurred during tensile tests are described below. Fig. 4 shows photographs of the typical failure types.

Failure type 1. Separation of the capillary from the solder occurs when the shear stress in the interface between the capillary and the solder is higher than the maximum allowable value. An approximation of the shear stress in this interface can be determined by dividing the maximum tensile force by the area on the shell of the capillary covered by solder. As the length of the capillary covered by solder was in the order of 1 mm this area is about 5 mm^2. The lowest measured tensile force for failure type 1 was 153 N, which results in a minimum shear stress of about 30 MPa. This is in the range of the minimum shear strength of solder on stainless steel of 25 MPa provided by the supplier (Fontargen). 25 MPa of shear stress on the wetted area on the capillary results in a total tensile force of 125 N. This would lead to a theoretical allowable pressure of $p_i = F_m/(\pi d^2/4) = 629$ bar on the connection, where d is the outer diameter of the capillary.

Failure type 2. Separation of the chromium layer from the silicon surface. The normal stress between the chromium layer and the silicon surface leads to failure. Normal stress is calculated by dividing the tensile load by the chromium surface area ($A = \pi d^2/4 = 19.63$ mm^2) with d being the diameter of the evaporated pad. The lowest measured tensile force before failure was 210 N, which results in a maximum allowable normal stress of 10.7 MPa for the undercoating. It is evident that this failure type is strongly dependent on the cleaning of the silicon surface before evaporation.

Failure type 3. The fracture of the Si/glass composite reaches the highest values for tensile loads. The stress situation is much more complex than in the former two failure types. The sample holder and hence its geometry plays an important role in the stress distribution around the soldered connection. The holder applies shear stress onto the sample and the Si/glass undergoes brittle failure. This indicates a higher mechanical strength of the connection than the Si/glass composite. For this failure type no information about the mechanical strength of the connection can be derived but conclusions about maximum handling loads which can be applied to the microreactor can be made.

The data in Fig. 5 show the three series of tensile tests at different temperatures. A large variation in all series and a slight decrease in maximum load with increasing temperature were seen. The large variation of failure load, especially for failure type 3, can be explained by the brittle behaviour of silicon and glass, which leads to a statistically distributed mechanical strength represented by a Weibull distribution [39]. A 1% probability of failure was calculated at a tensile load of 91.8 N at 60 °C.

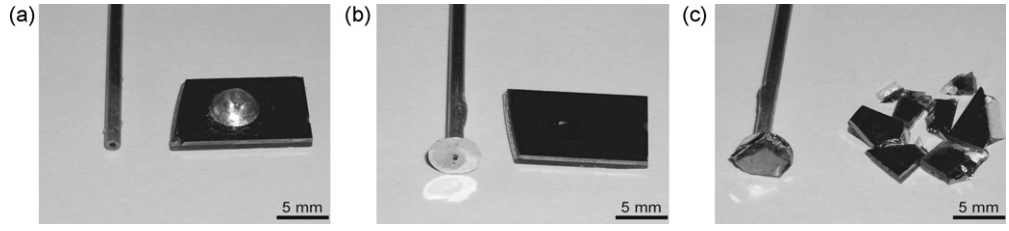

Fig. 4. Photographs of the three typical failure modes. (a) Failure type 1, separation of capillary from solder. (b) Failure type 2, separation of the Cr undercoating from Si. (c) Failure type 3, fracture of the Si/glass specimen.

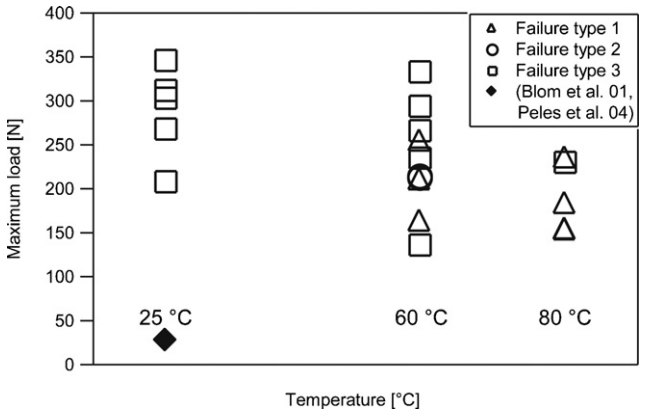

Fig. 5. Measured tensile loads of three series at different temperatures.

At higher temperatures, failure type 1 prevails. This is due to the difference in the coefficient of thermal expansion (CTE) of solder (CTE = $21.5 \times 10^{-6}\,K^{-1}$) and steel (CTE = $16.5 \times 10^{-6}\,K^{-1}$), which causes an additional thermal load on the connection as temperatures increase. The tensile test results indicate that the operating pressure and temperature region of the soldered microfluidic connection is suitable for the proposed operating conditions. The mechanical strength of the Si/glass reaction channel on the other hand can be estimated by beam theory [40]. The maximum applicable pressure is an inverse function of the square of the channel width. In this case the strength of the bond between the silicon and glass surface was the limiting factor, not the mechanical strength of either silicon or glass. At a pressure of 150 bar a maximum channel width of 515 μm is allowed without failure of the device.

A helium leak test was performed to measure the permeability of gas through the anodic bonding and the fluidic connection of the microreactor. No leaks were detected above a leak rate value of 10^{-11} mbar L/s. We therefore assumed a hermetic seal was formed by anodic bonding between the silicon and glass layer and that the soldered fluidic connection was tight. From polished cut micrographs of the soldered connection, the misalignment of the capillary relative to the microreactor inlet and outlet was analyzed to be about 180 μm. Pressure tests were conducted for over 8 h. The operating pressure was 140 bar and the temperature was 80 °C. No failure of the microreactor was observed during the entire experiment.

3.2. Hydrogenation of cyclohexene

3.2.1. Flow regime and residence time

A set of LIF experiments in an empty microchannel were conducted at pressures up to 50 bar to identify the flow regime and the liquid slug velocities in the microchannel. Superficial velocities were kept constant at $j_L = V_L^*/A = 0.0025$ m/s and $j_G = V_G^*/A = 0.1225$ m/s, where A is the cross-sectional area of the channel. The flow regime was identified as segmented gas–liquid flow with long gas bubbles extending the field of view of the LIF measurement setup (740 μm × 560 μm). In a set of 200 images recorded with a frame rate of 5 Hz, the liquid slug frequency was 0.1–0.4 Hz. Liquid slug lengths were in the range of 193–319 μm. This indicates that part of the fluid is flowing as wall flow through the microchannel. Double frame images with a time difference of 100 μs were taken from liquid slugs to calculate the velocities. The average liquid slug velocity measured was 0.15 ± 0.05 m/s. While increasing the system pressure, no significant change of the liquid slug length, liquid slug velocity or frequency was observed. Assuming the same velocity for both the liquid and gas phase in the microchannel, an average superficial velocity of both the phases of 0.13 m/s was calculated. This value was in the same range as the experimental results.

The measured liquid slug velocity was used to calculate mean liquid residence times of 0.17 s for an empty microchannel and 0.07 s for a randomly packed bed (porosity = 0.4) 26 mm in length. Since the actual liquid flow through the packed bed was not known as bypassing, axial dispersion and stagnant regions occur, the liquid residence time could only be estimated in the range of the above-calculated values. These residence times, combined with the recirculation motion in the liquid slug, allow us to safely assume the cyclohexene to be saturated with hydrogen at the entrance of the packed bed calculated by the diffusion length $x = \sqrt{2Dt}$, where D is the diffusion coefficient of hydrogen in cyclohexene and t is the diffusion time.

3.2.2. Reaction performance

The influence of pressure and temperature on the reaction rate was investigated, where the reaction rate r is defined as the moles of product formed per unit mass of catalyst per unit time. Fig. 6 shows the reaction rate as a function of the system pressure measured at the reactor outlet. The pressure drop across the packed bed was measured in all experiments to be between 0.4 and 0.5 bar. An increase of the reaction rate was seen at higher pressure due to an increase of the hydrogen solubility in cyclohexene.

The temperature dependence of the reaction rate is seen in Fig. 7. The conversions of the measured data ranged from 2.1 to 6.8% at 6 bar and 15–35.2% at 51 bar. Using the Arrhenius equation and the slope in Fig. 7(a) an activation energy E_A of 10.7 kJ/mol was calculated. Such small activation energies derived from the observed reaction rate indicate a mass transfer

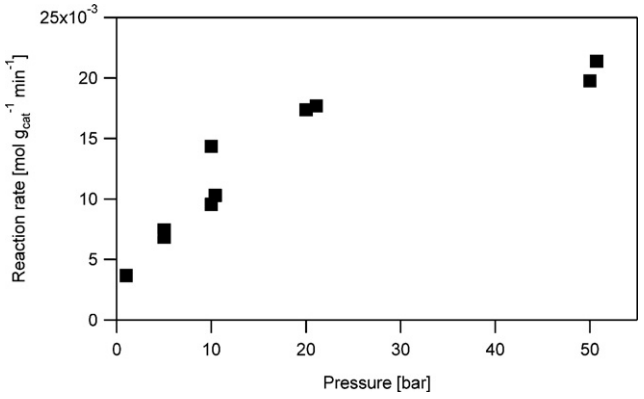

Fig. 6. Reaction rate for the hydrogenation of cyclohexene for pressures from 1 to 51 bar at ambient temperature. $V_L^* = 20$ μL/min and $V_G^* = 1 - 50$ mLn/min. At a pressure of 1 bar the reaction is conducted below stoichiometric conditions.

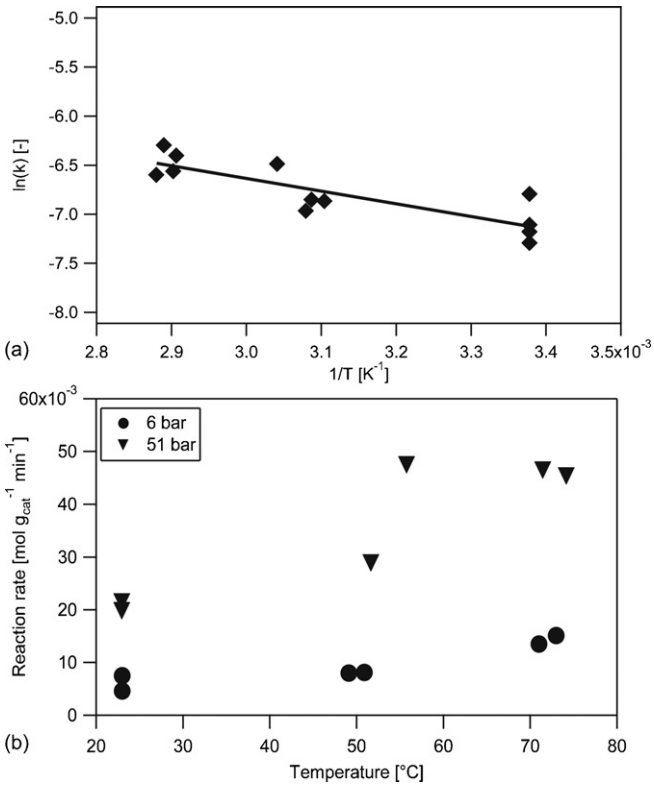

Fig. 7. (a) Arrhenius plot for the model reaction at $p = 5$ and 50 bar. Temperature was varied from 23 to 75 °C. The observed reaction order to hydrogen was 0.68. The linear regression equation is: $\ln(k) = -1291.5 \times (1/T) - 2.7609$ ($R^2 = 0.808$). (b) Reaction rate at different pressure and temperature.

limited reaction. An interpretation of mass transfer limitations was done by applying trickle-bed reactor theory [41]. The ratio of observed reaction rate to the mass transfer rate through the film surrounding the catalyst particle was calculated in the range of 1–6.8. This large film resistance for hydrogen strengthens the argument for a mass transfer limitation of the reaction in the segmented gas–liquid flow regime. A mass transfer limited reaction in the packed bed microreactor was also observed by Losey et al. [31].

In Fig. 7(b) the reaction rate as a function of temperature at two different pressures is shown. The reaction rate increases with temperature for two reasons. First the rate constant increases with temperature in the exponential term of the Arrhenius law, and second the solubility of hydrogen in the organic solvent increases with temperature, as it does with pressure. The deviations in reaction rate at the same reaction conditions could be explained by different flow paths through the packed bed and therefore a change in the mass transfer behaviour.

4. Conclusions

We demonstrated the feasibility of a Silicon/glass microreactor with soldered microfluidic connections for high-pressure and high-temperature chemical reactions. The microreactor was fabricated with standard photolithographic, dry etching and anodic bonding techniques. Metallic layers were evaporated on the silicon substrate in order to provide a wettable surface for the metallic solder. The mechanical analysis of the microreactor and its microfluidic connections showed a mechanical strength exceeding operating conditions of $T = 80$ °C and $p = 140$ bar. As a model reaction the exothermic gas-liquid-solid catalyzed hydrogenation of cyclohexene over Pd catalyst in a T-shaped packed bed microreactor was performed. The fluids were brought into contact in a static mixer followed by a mixing zone before entering the packed bed. LIF experiments confirmed a stable flow pattern for the investigated pressure range. The reaction rates at high pressures and temperatures showed an increase compared to earlier reported rates in microreactors. The reaction rate increased by about one order of magnitude at ambient conditions compared to conditions at 51 bar and 71 °C. A comparison with literature shows a mass transfer limitation of the reaction.

Acknowledgements

This work was supported by ETH Research Grant TH-32/05-2 and the Emil Barell foundation. The authors are grateful to F. Vogel and H.R. Scherrer for the valuable discussions and to the work of P. Hoffmann, B. Kramer and G. Kuhn at the workshop.

References

[1] J.J. Lerou, et al., Microfabricated minichemical systems: technical feasibility, DECHEMA Monographs 132, 1995, pp. 51–69.
[2] W. Ehrfeld, V. Hessel, H. Löwe, Microreactors: New Technology for Modern Chemistry, Wiley-VCH, Weinheim, 2000.
[3] K.F. Jensen, Microreaction engineering—is small better? Chem. Eng. Sci. 56 (2001) 293–303.
[4] S. Waelchli, P.R. von Rohr, Two-phase flow characteristics in gas–liquid microreactors, Int. J. Multiphase Flow 32 (2006) 791–806.
[5] F. Trachsel, et al., Measurement of residence time distribution in microfluidic systems, Chem. Eng. Sci. 60 (2005) 5729–5737.
[6] C.K. Fredrickson, Z.H. Fan, Macro-to-micro interfaces for microfluidic devices, Lab Chip 4 (2004) 526–533.
[7] B.L. Gray, et al., Novel interconnection technologies for integrated microfluidic systems, Sens. Actuators A 77 (1999) 57–65.
[8] A. Puntambekar, C. Ahn, Self-aligning microfluidic interconnects for glass- and plastic-based microfluidic systems, J. Micromech. Microeng. 12 (2002) 35–40.
[9] V.L. Spiering, et al., Novel microstructures and technologies applied in chemical analysis techniques, in: Proceedings of the 9th International Conference on Solid-State Sensors and Actuators (Transducers '97), Chicago, 1997.
[10] A.V. Pattekar, M.V. Kothare, Novel microfluidic interconnectors for high temperature and pressure applications, J. Micromech. Microeng. 13 (2003) 337–345.
[11] H. Andersson, et al., Micromachined flow-through filter-chamber for chemical reactions on beads, Sens. Actuators B 67 (2000) 203–208.
[12] Y. Peles, et al., Fluidic packaging of microengine and microrocket devices for high-pressure and high-temperature operation, J. Microelectromech. Syst. 13 (2004) 31–40.
[13] M.T. Blom, et al., Local anodic bonding of Kovar to Pyrex aimed at high-pressure, solvent-resistant microfluidic connections, J. Micromech. Microeng. 11 (2001) 382–385.
[14] V. Nittis, et al., A high-pressure interconnect for chemical microsystem applications, Lab Chip 1 (2001) 148–152.
[15] T.J. Yao, et al., Micromachined rubber O-ring micro-fluidic couplers, in: MEMS 2000, Miyazaki, Japan, 2000.
[16] H. Kestenbaum, et al., Silver-catalyzed oxidation of ethylene to ethylene oxide in a microreaction system, Ind. Eng. Chem. Res. 41 (2002) 710–719.

[17] A. Muller, et al., Fluidic bus system for chemical process engineering in the laboratory and for small-scale production, Chem. Eng. J. 107 (2005) 205–214.
[18] D.M. Ratner, et al., Microreactor-based reaction optimization in organic chemistry glycosylation as a challenge, Chem. Commun. (2005) 578–580.
[19] B.K.H. Yen, et al., A microfabricated gas–liquid segmented flow reactor for high-temperature synthesis: the case of CdSe quantum dots, Angew. Chem. Int. 44 (2005) 5447–5451.
[20] R.J. Madon, J.P. Oconnell, M. Boudart, Catalytic-hydrogenation of cyclohexene. 2. Liquid-phase reaction on supported platinum in a gradientless slurry reactor, AIChE J. 24 (1978) 904–911.
[21] E. Segal, R.J. Madon, M. Boudart, Catalytic-hydrogenation of cyclohexene. 1. Vapor-phase reaction on supported platinum, J. Catal. 52 (1978) 45–49.
[22] E.E. Gonzo, M. Boudart, Catalytic-hydrogenation of cyclohexene. 3. Gas-phase and liquid-phase reaction on supported palladium, J. Catal. 52 (1978) 462–471.
[23] P.C. Watson, M.P. Harold, Dynamic effects of vaporization with exothermic reaction in a porous catalytic pellet, AIChE J. 39 (1993) 989–1006.
[24] G. Wiessmeier, D. Honicke, Microfabricated components for heterogeneously catalysed reactions, J. Micromech. Microeng. 6 (1996) 285–289.
[25] K.K. Yeong, et al., Experimental studies of nitrobenzene hydrogenation in a microstructured falling film reactor, Chem. Eng. Sci. 59 (2004) 3491–3494.
[26] J. Kobayashi, et al., A microfluidic device for conducting gas–liquid–solid hydrogenation reactions, Science 304 (2004) 1305–1308.
[27] V. Hessel, S. Hardt, H. Löwe, Chemical Micro Process Engineering, Wiley-VCH, Weinheim, 2003.
[28] V. Hessel, et al., Gas–liquid and gas–liquid–solid microstructured reactors: contacting principles and applications, Ind. Eng. Chem. Res. 44 (2005) 9750–9769.
[29] L. Kiwi-Minsker, A. Renken, Microstructured reactors for catalytic reactions, Catal. Today 110 (2005) 2–14.
[30] G. Kolb, V. Hessel, Micro-structured reactors for gas phase reactions, Chem. Eng. J. 98 (2004) 1–38.
[31] M.W. Losey, M.A. Schmidt, K.F. Jensen, Microfabricated multiphase packed-bed reactors: characterization of mass transfer and reactions, Ind. Eng. Chem. Res. 40 (2001) 2555–2562.
[32] M.W. Losey, et al., Design and fabrication of microfluidic devices for multiphase mixing and reaction, J. Microelectromech. Syst. 11 (2002) 709–717.
[33] H. Surangalikar, X. Ouyang, R.S. Besser, Experimental study of hydrocarbon hydrogenation and dehydrogenation reactions in silicon microfabricated reactors of two different geometries, Chem. Eng. J. 93 (2003) 217–224.
[34] R.S. Besser, X. Ouyang, H. Surangalikar, Hydrocarbon hydrogenation and dehydrogenation reactions in microfabricated catalytic reactors, Chem. Eng. Sci. 58 (2003) 19–26.
[35] B. Desai, C.O. Kappe, Heterogeneous hydrogenation reactions using a continuous flow high pressure device, J. Combust. Chem. 7 (2005) 641–643.
[36] N. Yoswathananont, et al., Continuous hydrogenation reactions in a tube reactor packed with Pd/C, Chem. Commun. (2005) 40–42.
[37] M. Herskowitz, J. Wisniak, L. Skladman, Hydrogen solubility in organic liquids, J. Chem. Eng. Data 28 (1983) 164–166.
[38] V. Arunajatesan, et al., Fixed-bed hydrogenation of organic compounds in supercritical carbon dioxide, Chem. Eng. Sci. 56 (2001) 1363–1369.
[39] W. Weibull, A statistical distribution function of wide applicability, J. Appl. Mech. Trans. ASME 18 (1951) 293–297.
[40] M.T. Blom, et al., Failure mechanisms of pressurized microchannels, model, and experiments, J. Microelectromech. Syst. 10 (2001) 158–164.
[41] C.N. Satterfield, A.A. Pelossof, T.K. Sherwood, Mass transfer limitations in a trickle-bed reactor, AIChE J. 15 (1969) 226–234.